Phonon optimized interatomic potential for aluminum

Cite as: AIP Advances 7, 125022 (2017); https://doi.org/10.1063/1.5003158
Submitted: 03 September 2017 . Accepted: 13 December 2017 . Published Online: 21 December 2017

Murali Gopal Muraleedharan 📵, Andrew Rohskopf, Vigor Yang, and Asegun Henry









ARTICLES YOU MAY BE INTERESTED IN

Phonon properties and thermal conductivity from first principles, lattice dynamics, and the Boltzmann transport equation

Journal of Applied Physics 125, 011101 (2019); https://doi.org/10.1063/1.5064602

Interaction potentials for alumina and molecular dynamics simulations of amorphous and liquid alumina

Journal of Applied Physics 103, 083504 (2008); https://doi.org/10.1063/1.2901171

Nanoscale thermal transport

Journal of Applied Physics 93, 793 (2003); https://doi.org/10.1063/1.1524305







Phonon optimized interatomic potential for aluminum

Murali Gopal Muraleedharan,¹ Andrew Rohskopf,² Vigor Yang,¹ and Asegun Henry^{2,3,4,a}

¹School of Aerospace Engineering, Georgia Institute of Technology, Atlanta, GA 30332, USA ²George W. Woodruff School of Mechanical Engineering, Georgia Institute of Technology, Atlanta, GA 30332, USA

³Heat Lab, Georgia Institute of Technology, Atlanta, GA 30332, USA

⁴School of Materials Science and Engineering, Georgia Institute of Technology, Atlanta, GA 30332, USA

(Received 3 September 2017; accepted 13 December 2017; published online 21 December 2017)

We address the problem of generating a phonon optimized interatomic potential (POP) for aluminum. The POP methodology, which has already been shown to work for semiconductors such as silicon and germanium, uses an evolutionary strategy based on a genetic algorithm (GA) to optimize the free parameters in an empirical interatomic potential (EIP). For aluminum, we used the Vashishta functional form. The training data set was generated ab initio, consisting of forces, energy vs. volume, stresses, and harmonic and cubic force constants obtained from density functional theory (DFT) calculations. Existing potentials for aluminum, such as the embedded atom method (EAM) and charge-optimized many-body (COMB3) potential, show larger errors when the EIP forces are compared with those predicted by DFT, and thus they are not particularly well suited for reproducing phonon properties. Using a comprehensive Vashishta functional form, which involves short and long-ranged interactions, as well as three-body terms, we were able to better capture interactions that reproduce phonon properties accurately. Furthermore, the Vashishta potential is flexible enough to be extended to Al₂O₃ and the interface between Al-Al₂O₃, which is technologically important for combustion of solid Al nano powders. The POP developed here is tested for accuracy by comparing phonon thermal conductivity accumulation plots, density of states, and dispersion relations with DFT results. It is shown to perform well in molecular dynamics (MD) simulations as well, where the phonon thermal conductivity is calculated via the Green-Kubo relation. The results are within 10% of the values obtained by solving the Boltzmann transport equation (BTE), employing Fermi's Golden Rule to predict the phonon-phonon relaxation times. © 2017 Author(s). All article content, except where otherwise noted, is licensed under a Creative Commons Attribution (CC BY) license (http://creativecommons.org/licenses/by/4.0/). https://doi.org/10.1063/1.5003158

I. INTRODUCTION

Aluminum is one of the most abundant and most useful metals in the earth's crust. Micronsized aluminum powder has been routinely used in combustion, propulsion, and energy generation applications, due to its high energy density, low cost of extraction, and relative safety. The past decade, however, has marked a shift toward the use of nano-sized aluminum particles, which have large specific surface area and therefore higher reaction rates. Unfortunately, the formation of aluminum oxide on the particle surface reduces the rate of heat conduction between the heat release zone and the unburned reactants, which is a key process governing combustion wave propagation. For a spherical particle, for instance, the fraction of oxide increases from 6 to 47% as the size of



^aCorresponding Author Contact Information: Email: ase@gatech.edu, Phone: (404) 894-7514

the particle decreases from 30 to 3 nm.⁵ Therefore, the overall burning rates of nano-aluminum powders could be substantially diminished by the oxide surface, through reduced heat conduction rates.

The thermal conductivity of both bulk and nanoscale aluminum particles is dominated by electrons, and therefore Al should exhibit weak size effects at length scales of the order of 10's of nanometers. The thermal conductivity of aluminum oxide, on the other hand, is phonon dominated and is much lower than that of aluminum. It could, hence, become a predominant resistance to heat conduction as the combustion process proceeds towards completion. For such small particles, phonon boundary scattering may become important, since the oxide layer thickness can be \sim 2-3 nm, much smaller than the phonon mean free paths (MFP) in many other materials. Furthermore, not only the two solid phases, but also the interface between them probably plays a crucial role in heat conduction, and the interface may possibly be even more significant than the layers, in terms of resistance.

A series resistance circuit model can be used to estimate the total resistance, R of a nano-aluminum particle with oxide layer, and the contribution of each conductive resistance given as in Eq. 1.

$$R = 2R_{Al_2O_3} + 2R_{\text{int}} + R_{particle} \tag{1}$$

As a rough estimate based on phonon MFP spectra calculated for Al_2O_3 and the electron MFPs in Al_1^{12} we assume, $k_{Al} = 100$ W/m-K; $k_{Al2O3} = 5$ W/m-K for a 10 nm aluminum particle with a 3 nm oxidation layer. Lyeo *et al.*¹³ report results for the temperature dependence of interfacial conductance of Al/Al_2O_3 measured using the time-domain thermoreflectance (TDTR) method. They obtained a room temperature interfacial conductance of ~200 MW m⁻² K⁻¹. Using this data, the interfacial resistance R_{int} is 5×10^{-9} m²K/W, and our simplified estimate suggests that the interfacial conductance is likely to dictate ~ 90% of the total resistance. We therefore expect that the interface will be dominant, the contribution from the oxide layer is < 10%, and the Al comprises < 1%. It is theorized, and there is some evidence that suggests, that electrons also make a negligible contribution to the interfacial resistance, ¹⁴ and therefore the phonons are most critical.

Classical molecular dynamics (MD) can be used to study phonons and predict both interfacial conductance¹⁵ and phonon thermal conductivity. ¹⁶ *Ab initio* methods such as density functional theory (DFT)¹⁷ may also be used, but they are limited by the system size. They also do not decompose the force on atoms in terms of contributions from other atoms; that is, only the total force on atoms results, since the charge density is not easily partitioned into individual atom contributions. Formalisms that provide phonon mode-level information on thermal conductivity¹⁸ and interfacial conductance¹⁹ require force decomposition, so it is not clear how such formalisms could be used in conjunction with DFT.

One promising approach to studying phonon physics is to develop a phonon optimized interatomic potential (POP) that can be used in MD simulations.²⁰ The most widely used potential for Al is the embedded atom method (EAM);²¹ the charge optimized many body (COMB3) potential has also recently been used to model Al.^{22,23} However, these potentials were not specifically designed or optimized to describe phonons, and it is not known how well these potentials will reproduce ab initio MD trajectories and subsequent phonon-related properties. In theory, the complexity in common potential forms should be capable of capturing phonons accurately, but to better quantify the extent to which the existing potentials (EAM and COMB3) can describe phonons, we compare their predicted forces with forces obtained from DFT results for supercells, where the atoms have been randomly displaced from their equilibrium lattice sites. As a quick test, we performed self-consistent field (SCF) calculations on Al (full details given in the methodology section), and the total force errors were compared with those of predictions by EAM²¹ and COMB3,²² using a FCC supercell of Al consisting of 32 atoms. The crystal was first relaxed, then random displacements (maximum = 0.01 Å and RMS = 0.0062 Å) were given to each atom and forces were evaluated. Comparing the forces from the calculations predicted by EAM and COMB3 potentials with the DFT results, the average error in forces for EAM was ~ 52\% and ~ 48\% for COMB3. Accurate force predictions are important for predicting phonon properties, but it is not well understood what value of force error can be tolerated and still yield reasonable phonon properties. Prior works^{20,24} on the development of POP for crystalline silicon and germanium suggest ~10% force error is satisfactory.

In this work, we present a POP for Al based on a training set consisting entirely of DFT calculations. Initial work by Rohskopf *et al.*²⁰ showed that the POP methodology can work for semiconductors such as Si and Ge, and suggested²⁴ that the method is general and can be extended to other materials/classes. Here we apply the POP methodology to a metal (Al) and seek to determine if the POP approach can properly reproduce the phonon contributions to thermal conductivity for Al. Training datasets to sample the phase space were generated from DFT calculations, and consist of five key properties, namely total forces and stresses, energy vs. volume, and harmonic and cubic force constants. As for Si and Ge, a genetic algorithm^{25,26} based optimization routine was used to search the space of fitting parameters. The Vashishta²⁷ functional form was chosen to describe the potential because it consists of short and long-range interactions, and three-body terms to capture phonon interactions. Since the functional form is sufficiently flexible to describe both Al and Al₂O₃, in a future study the interfacial conductance between the two phases can be studied in detail.

II. METHODOLOGY

A. The Vashishta potential functional form

The Vashishta potential has previously been used in MD simulations for thermal transport property evaluations;²⁸ it was originally developed for silicon carbide²⁷ and has been extended to Al₂O₃.²⁹ The potential is fairly comprehensive, and may be parameterized for describing the Al/Al₂O₃ interface in future, with the goal of describing each bulk material as well as the interface, all with a single functional form – albeit with different parameters for Al interactions in each phase (i.e. an Al atom in metallic Al will likely be treated as a different species from Al in Al₂O₃). The Vashishta functional form expresses interaction potential energy consisting of two and three-body terms:

$$V = \sum_{i < j} V_{ij}^{(2)}(r_{ij}) + \sum_{i,j < k} V_{ijk}^{(3)}(r_{ij}, r_{ik})$$
 (2)

The two-body term includes steric-size effects, Coulomb interactions, charge-induced dipole, and van der Waals interactions, and can be written as:

$$V_{ij}^{(2)}(r) = \begin{cases} \frac{H_{ij}}{r^{\eta_{ij}}} + \frac{Z_i Z_j}{r} e^{-\frac{r}{\chi}} - \frac{D_{ij}}{2r^4} e^{-\frac{r}{\xi}} - \frac{W_{ij}}{r^6}, r \le r_c, \\ 0, r > r_c. \end{cases}$$
(3)

It is truncated at r_c and the shifted potential can be described as:

$$V_{ij}^{(2,shifted)}(r) = \begin{cases} V_{ij}^{(2)}(r) - V_{ij}^{(2)}(r_c) - (r - r_c) \left[dV_{ij}^{(2)}(r) / dr \right]_{r = r_c}, r \le r_c, \\ 0, r > r_c. \end{cases}$$
(4)

The three-body term is a product of spatial and angular dependent components,

$$V_{ijk}^{(3)}(r_{ij}, r_{ik}) = R^{(3)}(r_{ij}, r_{ik})P(\theta_{jik})$$
(5)

$$R^{(3)}(r_{ij}, r_{ik}) = B_{jik} \exp\left(\frac{\gamma}{r_{ij} - r_o} + \frac{\gamma}{r_{ik} - r_o}\right) \Theta\left(r_o - r_{ij}\right) \Theta\left(r_o - r_{ik}\right)$$
(6)

$$P^{(3)}(\theta_{jik}) = \frac{\left(\cos\theta_{jik} - \cos\overline{\theta}_{jik}\right)^2}{1 + C_{jik}\left(\cos\theta_{jik} - \cos\overline{\theta}_{jik}\right)^2} \tag{7}$$

In this study, among the 13 independent parameters, 12 parameters H, η , χ , D, ξ , W, r_c , B, γ , r_0 , C, and $\cos \overline{\theta}_{jik}$ need to be optimized. The charges Z_i can be set to zero in the aluminum crystal, since it is charge neutral.

B. Genetic algorithm based optimization

With 12 independent fitting parameters, the corresponding 12 dimensional optimization problem could easily fail if local minima-based optimization strategies are used. Therefore, a genetic algorithm (GA) based optimization technique is used to obtain the parameters. A GA, with its metaheuristic approach, mimics natural selection, providing a more complete and efficient exploration of the multi-dimensional parameter space. ^{25,30,31} The basic approach of a GA is to evolve a potential set of randomly generated candidate solutions (termed "individuals") towards better solutions via multiple evolutionary stages (termed "generations") by minimizing an objective function. The objective function, *Z* is a measure of the error between the training set values for each configuration and the values for a candidate set of fitting parameters, and is given as:

$$Z = w_f z_f + w_e z_e + w_s z_s + w_{ifc2} z_{ifc2} + w_{ifc3} z_{ifc3},$$
(8)

where, z represents generalized errors, and w represents the weights. The subscripts f, e, s, ifc2 and ifc3 represent force, energy, stress, harmonic force constant, and cubic force constants. The errors are given by Rohskopf et al.²⁰ as:

$$z_{f} = \frac{\sum_{j}^{M} \sum_{i}^{N} \|\vec{F}_{ij}^{DFT} - \vec{F}_{ij}^{EIP}\|^{2}}{3MN \sum_{j}^{M} \sum_{i}^{N} \|\vec{F}_{ij}^{DFT}\|^{2}}$$
(9)

where \vec{F}_{ij}^{DFT} is the *ab initio* Hellman-Feynman force on atom *i* in configuration *j* and \vec{F}_{ij}^{EIP} is the force predicted by the potential. The error is summed over all *N* atoms and *M* configurations, and is normalized by the number of forces and sum of *ab initio* forces. The error for energy z_e is given by

$$z_{e} = \frac{\sum_{j}^{M} (E_{j}^{DFT} - E_{j}^{EIP})^{2}}{M \sum_{j}^{M} (E_{j}^{DFT})^{2}}$$
(10)

where E_j^{DFT} is the *ab initio* energy and E_j^{EIP} is the energy predicted by the fitted potential. Energy is referenced to the energy of the fully relaxed equilibrium configuration. Emphasis is placed on reproduction of the shape of the energy vs. volume curve, and therefore, the energy is described as an energy difference $E_j = \varepsilon_j - \varepsilon_{coh}$, where ε_j is the total potential energy and ε_{coh} is the total potential energy of the DFT equilibrium configuration with the equilibrium cell dimensions. With this definition for energy, the energy of the relaxed/minimized structure will always be zero. The error for supercell stress z_s is then given by,

$$z_{s} = \frac{\sum_{j}^{M} \sum_{k}^{6} \left\| \sigma_{jk}^{DFT} - \sigma_{jk}^{EIP} \right\|^{2}}{6M \sum_{j}^{M} \sum_{k}^{6} \left\| \sigma_{jk}^{DFT} \right\|^{2}}$$
(11)

where σ_{jk}^{DFT} and σ_{jk}^{EIP} are the k^{th} symmetric ab initio and EIP stress tensor components of the j^{th} configuration, respectively. The sum over k stress tensor components considers the six symmetric components σ_{xx} , σ_{yy} , σ_{zz} , σ_{xy} , σ_{xz} , and σ_{yz} . Both of these quantities are important for stability and proper dynamics, which depend strictly on the shape of the energy-volume curve. Fitting of IFCs is accomplished by addition of another error component, z_{ijc}^o , where o is the order of the IFC being fit. The IFC error component is given by:

$$z_{e} = \frac{\sum_{n}^{P} (\phi_{n}^{DFT} - \phi_{n}^{EIP})^{2}}{P \sum_{n}^{P} (\phi_{n}^{DFT})^{2}}$$
(12)

where P is the number of IFCs and ϕ_n^{DFT} and ϕ_n^{EIP} are the i^{th} order ab initio and EIP IFCs, respectively. The training set consists of the properties being optimized, which may be obtained from experimental or ab initio results. In the present work, only ab initio DFT results are used to generate the training set, as described in Section III C. After each generation, the individuals with the least error (the lowest objective function value), termed the elite population, are stochastically selected and evolved to the next generation after experiencing some 'mutation' and 'crossover'. In a GA, a set of EIP parameters is termed and individual and individuals are represented as binary strings. When represented as a single binary string, one or more bits can be flipped at random to produce a random "mutation". 'Crossover' refers to the mixing of multiple individuals to obtain a new 'child' solution.

Here we start with 1200 individuals (that is, 1200 randomly generated parameter sets with 12 parameters each). A group of 1200 individuals is termed a trial, and a trial is allowed to evolve for 250 generations with an elite population of 10%. The elite population is the group of individuals that exhibited the lowest value for the objective function in that generation. The rest of the population is randomly selected and grouped with the elites so that 50% of the total population is mixed with these better performing parameter sets, and they experience crossover and mutation. For a particular generation, this 50% of solutions are termed the "parents". The parents first undergo a crossover operation, where a single random crossover point in the string is chosen for two parent solutions. The binary strings that represent the decimal parameter values of a parent solution are split at the crossover point, and all the strings beyond this point are swapped with corresponding strings from the other parent. This recombination results in a "child" solution that then has a randomly chosen mixture of the two parent binary representations. The next step is to apply the mutation operation, where the binary strings representing decimal values of each "child" solution experience random perturbations from "0" to "1" or vice versa. The mutation operation randomly perturbs existing parameters and it allows the optimization process to explore the full parameter space, reducing the chance of getting stuck in a local minimum. This means that only the top 10% of each generation survive and the remaining 90% of the individuals in the next generation are generated through the aforementioned process.

The objective function value, termed the "fitness", of each parameter set is then evaluated from the error obtained with respect to each fitted quantity in the DFT training set. The properties, such as individual atom forces and super cell stresses, are calculated using the LAMMPS³² open source code as a shared library with the POP code.²⁰ The respective weights for the objective function components are given in Table I. The best individuals or the elites in each generation, are then used to seed the next generation. In the end a single best solution is not necessarily obtained, but rather many unique solutions with nearly degenerate objective function values are obtained. Here, the best 200 parameter sets were selected for statistical analysis and the resulting parameters cover the ranges given in Table II, which is also reported in the supplementary material.

TABLE I. Fitting properties and weights.

Properties	Weight
Total Force	0.1
Energy vs. Volume	0.3
Stress	0.3
Harmonic force constant (2FC)	0.2
Cubic force constant (3FC)	0.1
Total	1.0

TABLE II.	Input and of	output paramete	er ranges, fracti	on of sear	ch space	obtained	as output,	and the s	specific va	lues obtained
for the Vasl	hishta-56 pa	rameter set.								

Parameter	Range	Output Range	Fraction,%	Vashishta-56
H, eVÅ ^η	$[10^{-2} - 0.5 \times 10^{3}]$	[62.68-188.60]	25.18	153.62840
η	$[10^{-5}-10^{1}]$	[4.99-6.21]	12.20	6.02
χ, Å	$[10^{-2}-10^{1}]$	[0.09-10]	99.10	5.06
D, eVÅ ⁴	$[10^{-5}-10^{1}]$	[0.02-5]	99.60	4.08
ξ, Å	$[10^{-5}-0.5\times10^{2}]$	[0.45-49.92]	98.94	1.83
W, eVÅ ⁶	$[10^{-5} - 0.5 \times 10^{1}]$	[0.19-4.99]	96.00	0.6932
r_c , Å	$[10^{-5}-10^{1}]$	[5.42-10]	45.80	9.64
B, eV	[10-20]	[10.1-20]	99.00	15.59
γ, Å	$[10^{-5}-10^{3}]$	[0.13-4.81]	46.80	2.16
r_0 , Å	$[10^{-5}-0.5\times10^{1}]$	[0.08-3.56]	69.60	0.34
\tilde{C}	$[10^{-5}-3x10^{1}]$	[0.01-29.66]	98.83	28.59
$\cos \overline{\theta}_{jik}$	[-1,1]	[-1-1]	100	0.0

C. Training data set

Appropriate training datasets that sufficiently sample the relevant phase space were generated from DFT calculations. The DFT calculations were performed employing the local density approximation (LDA) for the exchange-correlation functional, and the normconserving Perdew-Zunger³³ scalar relativistic pseudopotential was used to describe the core electrons. The projector-augmented wave formalism was implemented in QUANTUM ESPRESSO (QE)³⁴ with a plane wave energy cutoff of 750 eV. The Brillouin zone was sampled using 4x4x4 uniform (Monkhorst-Pack) k-point grids. For the self-consistent field (SCF) calculations, the electron energy convergence threshold was set $1x10^{-7}$ eV, and for the initial structural optimization, the force/atom convergence threshold was set to $1x10^{-4}$ eV/Å.

To further validate the accuracy of the DFT calculations before proceeding to phonon optimization, we used the open-source ALAMODE code, ³⁵ which is useful for calculating the harmonic and anharmonic force constants from DFT data, and also facilitates the calculation of dispersion relations and the phonon DOS. The phonon DOS was calculated using a 4x4x4 mesh resolution, and dispersion relations were extracted using a fine 150 one-dimensional grid points along each phonon branch. The phonon BTE is solved under a relaxation time approximation (RTA) using a 30x30x30 grid, which produces converged phonon thermal conductivity values that can be compared with our results and with experimental data.

A total of 100 configurations (26 for force constant fitting + 74 for other properties) were used in the training set. Note that the number of configurations is significantly lower than those required for neural network potentials (NNP), Gaussian approximated potentials (GAP), or the spectral neighbor analysis potential (SNAP). In addition, comparing the speeds of these potentials when implemented in LAMMPS, GAP and SNAP are 10 times slower whereas NNP is \sim 4 times slower than the much simpler Vashishta potential. These are significant computational savings by comparison to more complex potentials, which is one of the key advantages of the POP approach, where the goal is explicitly to study phonons rather than attempting to describe the entire phase/configuration space.

III. RESULTS AND DISCUSSION

A. Parameter optimization

Table II shows the ranges allowed for the fitting parameters in the Vashishta functional form, where 12 parameters were optimized. The atomic charges in the Coulomb term of the potential were assigned a value of zero, since Al is monatomic. The ranges explored for each parameter are given in the second column and the range of values for each parameter that appear in the best 200 solutions are given in the third column. Initial inputs were chosen over a much broader range, which was manually narrowed down to reduce the search space once several solutions emerged. Column 4 gives

the fraction of input parameter range comprised by the solutions. Since there are many solutions, it would be cumbersome to represent all of them in tables as is common practice.^{20,22} Instead, we have provided LAMMPS input files that refer to specific solutions by a reference index (Vashishta-1, 2, etc.) in the supplementary material. Among these sets of solutions, some may be transferable to describe other properties, such as surfaces, defects, or alloys, although transferability is neither guaranteed, nor an objective of the approach.

The statistics give a sense of how much diversity there is in the solutions. For example, if a parameter has a narrow range, then in all the solutions this parameter was essentially fixed at a nearly unique optimal value. On the other hand, if a parameter varies drastically, the solutions span a wide range and are not degenerate in representation, despite the fact that they all reproduce the forces well and have nearly degenerate objective function values.

Figure 1 shows the error in forces on atoms. The minimum error is $\sim 32\%$, and the maximum is $\sim 45\%$, excluding a few outliers. While Rohskopf *et al.*²⁰ suggest that force error of $\sim 10\%$ is to be aimed for, it is important to investigate whether the solutions ensure a fair prediction of phonon properties. Therefore, in the following sections, the accuracy of the fitted potential with the lowest force error (i.e., Vashishta-56) is compared against the results of EAM, COMB3, and DFT results.

B. Thermal conductivity accumulation plots

In order to test the accuracy of the fitted potential, it is important to evaluate its efficacy in calculating phonon thermal conductivity. Based on the Wiedemann-Franz law, the thermal conductivity of Al is dominated by electrons (>90%), and it is also quite high (> 200 W/m-K). Since it is dominated by electrons, this puts a large degree of uncertainty on the phonon contribution, if it is to be inferred from experiments. Phonon thermal conductivity can therefore be expected to be less than 20 W/m-K. Here, we calculate the phonon thermal conductivity by solving the phonon Boltzmann transport equation (BTE) under relaxation time approximation (RTA). Solution of BTE was performed using ALAMODE.³⁵ An atomic displacement of 0.01 Å was used for perturbing the atoms from equilibrium positions. Prior researchers 16,36 have also made similar attempts to calculate thermal conductivity of Al, but do not report the magnitude of atomic displacements used. Jain and McGaughey¹⁶ report a thermal conductivity of ~8 W/m-K at 300 K, whereas Wang et al.³⁶ predict the phonon thermal conductivity to be ~4.8 W/m-K. Our results, however, indicate a thermal conductivity of ~ 1 W/m-K at 300 K. Although there is disparity in these three computed values, additional calculations showed that this is likely due to the difference in atomic displacements used in the DFT calculations. Furthermore, because of the large degree of uncertainty associated with the phonon contributions, all the values are arguably consistent with the Wiedemann-Franz Law, since they are all < 20 W/m-K.

The cumulative thermal conductivity (thermal conductivity vs. phonon mean free path) or the accumulation plot is obtained, as shown in Fig. 2. The figure compares results from DFT, Vashishta-56, EAM and COMB3 at 300 K. As shown in the figure, the POP Vashishta-56 gives excellent agreement

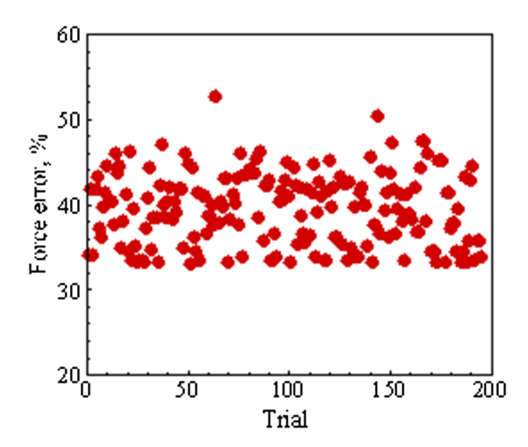


FIG. 1. Error (%) in forces on atoms for the various sets (trials) of Vashishta potential parameters.

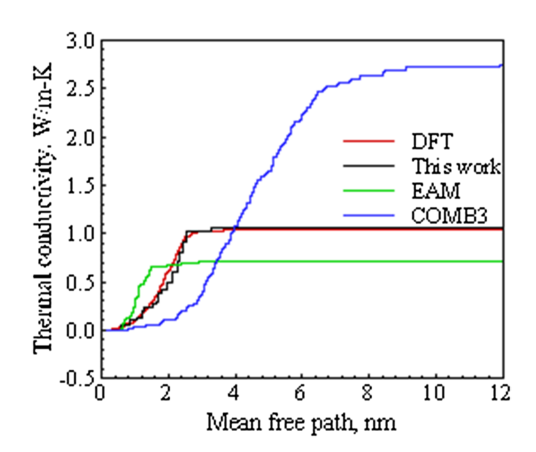


FIG. 2. Thermal conductivity accumulation plot estimated using Vashishta-56 (this work) compared with the DFT (RTA) and predictions of, EAM, and COMB3.

with DFT results. While COMB3 over-predicts the results by about 140% and predictions from the EAM potential are about 40% lower than the DFT results. These potentials are unable to reproduce the thermal conductivity accumulation with respect to the phonon mean free paths, which indicates that they may not be suited for describing phonons. However, the Vashista-56 potential exhibits good agreement in both the total value of thermal conductivity and the accumulation function.

C. Phonon density of states

In addition to the accumulation plots, phonon densities of states (DOS) were also calculated using the different potentials and comparing with the DFT results, as shown in Fig. 3. As can be seen from the figure, phonon DOS predicted by our potential has a better agreement with the DFT results in terms of the proximities of the peaks. The EAM and COMB3 potentials exhibit good qualitative agreement, but the actual peaks in frequencies are off by more than 50% in both height and location.

D. Phonon dispersion relations

Phonon dispersion relations represent the phonon branches. It has been shown²² that COMB3 and EAM predict dispersion relations well. Figure 4 shows that the Vashishta-56 potential is also quite satisfactory when compared with DFT and experimental³⁷ results. In theory, an improved functional form such as a Taylor expansion may offer sufficient flexibility to capture all the necessary force constants, particularly for the non-first nearest neighbors. It should also be noted that DFT results can

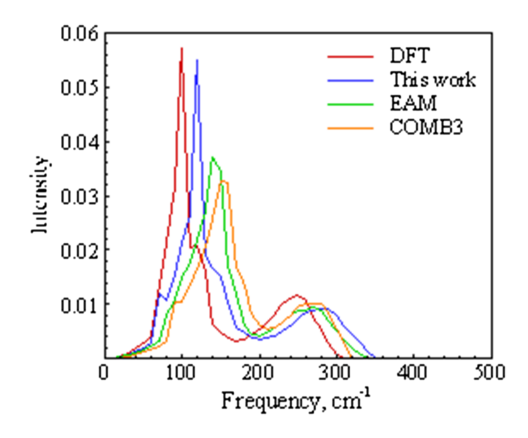


FIG. 3. Phonon density of states (DOS) calculated by Vashishta-56 (this work), EAM, and COMB3 compared with DFT results.

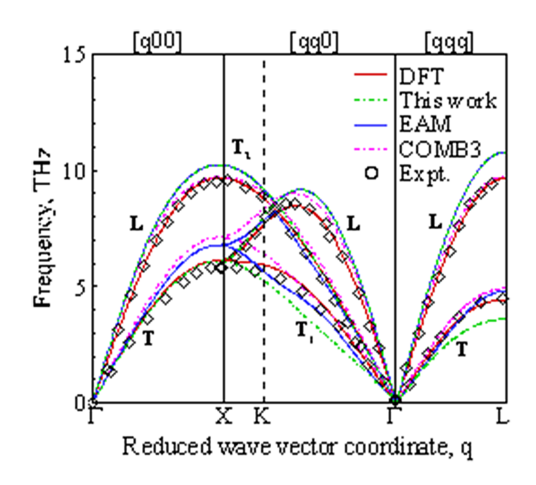


FIG. 4. Phonon dispersion relations calculated using Vashishta-56 (this work), EAM, and COMB3 compared with DFT and experimental results.³⁷

vary marginally with the pseudopotential used to describe core electrons, but generally the quantitative and qualitative trends have been captured with high levels of accuracy.

E. Green-Kubo thermal conductivity calculations

Having shown that the Vashishta-56 potential captures the basic phonon properties from the various ALAMODE calculations, it is important to test its applicability in MD simulations. Using Vashishta-56, molecular dynamics simulations were performed using LAMMPS, 32 to test predictions of thermal conductivity (k), using the Green-Kubo relation given by:

$$k = \frac{1}{k_B T^2} \int_{0}^{\infty} \frac{\left\langle \vec{S}(t) . \vec{S}(0) \right\rangle}{3} dt, \tag{13}$$

where k_B is the Boltzmann constant and T is temperature. The heat current vector S was derived by Hardy.³⁸

$$\vec{S} = \frac{1}{V} \left\{ \sum_{i} \frac{\vec{p}_{i}}{m_{i}} \left(\frac{p_{i}^{2}}{2m_{i}} + U_{i} \right) + \sum_{i} \sum_{i} \left(\frac{\partial U_{ij}}{\partial r_{i}} . \vec{v}_{i} \right) \vec{r}_{ij} \right\}, \tag{14}$$

where V is the volume, p is momentum, m is the atomic mass, U is the potential energy, v is the velocity, and r is the position of atoms represented by i and j. To test for stability, we tried different ensembles and thermostats to make sure the crystal preserved its lattice stability throughout the calculation without any significant deviations in energy or structure. For the thermal conductivity calculation, as a first step, the energy of a FCC crystal with 256 atoms was minimized by the conjugate-gradient (CG) method with a relative tolerance of 1×10^{-4} and 1×10^{-6} for energy and forces respectively, and the system was then equilibrated in the NPT ensemble for 10 ps. A time-step size of 0.1 fs was used and the Green-Kubo calculations were performed for another 100 ps with a correlation length of 1 ps. The crystal size of 256 atoms and correlation time of \sim 1 ps were determined to be sufficient after testing for convergence.

The temperature dependency of lattice thermal conductivity of the FCC Al crystal was compared with the results from the solution of the phonon Boltzmann transport equation. Results of the calculations are presented in Fig. 5. For each temperature, ~ 35 independent results were averaged; the error bars correspond to the standard deviation amongst the independent results. As the figure shows, there is again a good agreement with the BTE results in the temperature range considered. The maximum deviation, $\sim 10\%$, is observed at 400 K. For all the other temperatures, the deviation is well within our goal of 10%. This suggests that POP Vashishta-56 can be used to simulate the phonons in Al, with fidelity.

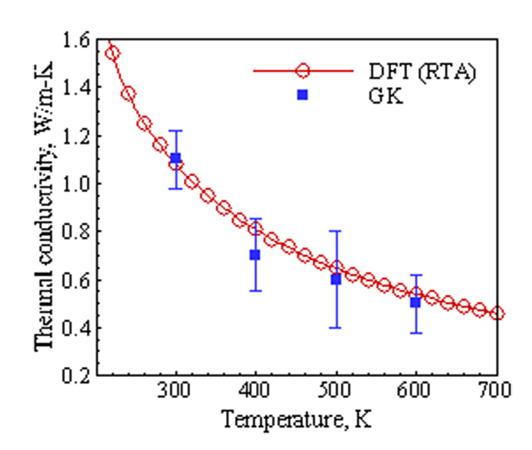


FIG. 5. Temperature dependency of thermal conductivity calculated using Green-Kubo relations compared with DFT (RTA) results.

IV. CONCLUSIONS

In this work, phonon-optimized potential (POP) for aluminum has been developed, and this is the first application of this method to a metal. The POP methodology was previously validated for silicon and germanium, and now has been extended to aluminum via the Vashishta functional form, resulting in approximately 200 solutions of interest. The functional form and the parameter sets can be readily used in MD simulations using LAMMPS software. The phonon properties predicted by Vashishta-56 align well with the results from DFT calculations, and the force error is $\sim 32\%$, which is somewhat lower than previous EAM and COMB3 potentials. Nonetheless, despite the seemingly large force error, the Vashishta-56 potential is able to accurately reproduce the phonon-phonon interactions, as indicated by the excellent agreement between the thermal conductivity accumulation plots in Fig. 2. When using MD, the thermal conductivity calculated by the Green-Kubo method is within 10% of the BTE-RTA results. In the future, this same approach can be extended to aluminum oxide (Al $_2$ O $_3$) and to the interface between Al and Al $_2$ O $_3$, which is of interest to the combustion community.

SUPPLEMENTARY MATERIAL

See supplementary material for the open-source POP code and manual are located at www.pops.gatech.edu. The parameters for potentials used in this study are attached as separate files as supplementary material.

ACKNOWLEDGMENTS

This work was sponsored by the US Air Force Office of Scientific Research under contract no. FA-9550-13-1-0004. Support and encouragement provided by Dr. Mitat A. Birkan is gratefully acknowledged. An NSF Career award (1554050) to A. H. is also acknowledged.

- ¹ V. Yang, Solid Propellant Chemistry Combustion and Motor Interior Ballistics 1999, Vol. 185 (AIAA, 2000).
- ² D. Sundaram, V. Yang, and R. A. Yetter, Progress in Energy and Combustion Science **61**, 293 (2017).
- ³ D. S. Sundaram, P. Puri, and V. Yang, Combustion and Flame 169, 94 (2016).
- ⁴ Y. Huang, G. A. Risha, V. Yang, and R. A. Yetter, Combustion and Flame 156, 5 (2009).
- ⁵ D. Sundaram, V. Yang, and V. Zarko, Combustion, Explosion, and Shock Waves **51**, 173 (2014).
- ⁶ G. Chen, Nanoscale energy transport and conversion: A parallel treatment of electrons, molecules, phonons, and photons (Oxford University Press, 2005).
- ⁷ Z. M. Zhang, *Nano/microscale heat transfer* (McGraw-Hill, New York, 2007).
- ⁸ A. Mayadas, Journal of Applied Physics **39**, 4241 (1968).
- ⁹ K. T. Regner, D. P. Sellan, Z. Su, C. H. Amon, A. J. McGaughey, and J. A. Malen, Nature Communications 4, 1640 (2013).
- ¹⁰ Y. Ju and K. Goodson, Applied Physics Letters **74**, 3005 (1999).
- ¹¹ H. J. Maris, Philosophical Magazine 9, 901 (1964).
- ¹² D. Gall, Journal of Applied Physics **119**, 085101 (2016).
- ¹³ H.-K. Lyeo and D. G. Cahill, Physical Review B 73, 144301 (2006).

- ¹⁴ J. Olson and R. Pohl, Journal of Low Temperature Physics **94**, 539 (1994).
- ¹⁵ Y. Chalopin, K. Esfarjani, A. Henry, S. Volz, and G. Chen, Physical Review B 85, 195302 (2012).
- ¹⁶ A. Jain and A. J. McGaughey, Physical Review B **93**, 081206 (2016).
- ¹⁷ R. G. Parr, in *Horizons of Quantum Chemistry* (Springer, 1980), p. 5.
- ¹⁸ W. Lv and A. Henry, New Journal of Physics **18**, 013028 (2016).
- ¹⁹ K. Gordiz and A. Henry, New Journal of Physics **17**, 103002 (2015).
- ²⁰ A. Rohskopf, H. R. Seyf, K. Gordiz, T. Tadano, and A. Henry, NPJ Computational Materials 3, 1 (2017).
- ²¹ M. S. Daw and M. I. Baskes, Physical Review B **29**, 6443 (1984).
- ²² K. Choudhary, T. Liang, A. Chernatynskiy, Z. Lu, A. Goyal, S. R. Phillpot, and S. B. Sinnott, Journal of Physics: Condensed Matter 27, 015003 (2014).
- ²³ T. Liang, T.-R. Shan, Y.-T. Cheng, B. D. Devine, M. Noordhoek, Y. Li, Z. Lu, S. R. Phillpot, and S. B. Sinnott, Materials Science and Engineering: R: Reports 74, 255 (2013).
- ²⁴ A. Rohskopf, H. R. Seyf, K. Gordiz, and A. Henry, arXiv preprint arXiv:1610.02353 (2016).
- ²⁵ D. A. Coley, An introduction to genetic algorithms for scientists and engineers (World Scientific Publishing Co Inc, 1999).
- ²⁶ J. D. Schaffer, D. Whitley, and L. J. Eshelman, in Combinations of genetic algorithms and neural networks: A survey of the state of the art, 1992 (IEEE), p. 1.
- ²⁷ P. Vashishta, R. K. Kalia, A. Nakano, and J. P. Rino, Journal of Applied Physics **101**, 103515 (2007).
- ²⁸ M. G. Muraleedharan, D. S. Sundaram, A. Henry, and V. Yang, Journal of Physics: Condensed Matter **29**, 155302 (2017).
- ²⁹ P. Vashishta, R. K. Kalia, A. Nakano, and J. P. Rino, Journal of Applied Physics 103, 083504 (2008).
- ³⁰ A. Turing, IEEE Intelligent Systems **2** (1950).
- ³¹ D. B. Fogel, IEEE Transactions on Neural Networks 5, 3 (1994).
- ³² S. Plimpton, Journal of Computational Physics **117**, 1 (1995).
- ³³ J. P. Perdew and A. Zunger, Physical Review B **23**, 5048 (1981).
- ³⁴ P. Giannozzi, S. Baroni, N. Bonini, M. Calandra, R. Car, C. Cavazzoni, D. Ceresoli, G. L. Chiarotti, M. Cococcioni, and I. Dabo, Journal of Physics: Condensed Matter 21, 395502 (2009).
- ³⁵ T. Tadano, Y. Gohda, and S. Tsuneyuki, Journal of Physics: Condensed Matter **26**, 225402 (2014).
- ³⁶ Y. Wang, Z. Lu, and X. Ruan, Journal of Applied Physics **119**, 225109 (2016).
- ³⁷ R. T. Stedman and G. Nilsson, Physical Review **145**, 492 (1966).
- ³⁸ R. J. Hardy, *Physical Review* **132**, 168 (1963).